

See discussions, stats, and author profiles for this publication at: <https://www.researchgate.net/publication/263946643>

PVDF/Nanosilica Dual-Layer Hollow Fibers with Enhanced Selectivity and Flux as Novel Membranes for Ethanol Recovery

ARTICLE *in* INDUSTRIAL & ENGINEERING CHEMISTRY RESEARCH · JANUARY 2012

Impact Factor: 2.59 · DOI: 10.1021/ie202116h

CITATIONS

26

READS

47

2 AUTHORS, INCLUDING:



Tai-Shung Chung

National University of Singapore

727 PUBLICATIONS 19,578 CITATIONS

[SEE PROFILE](#)

PVDF/Nanosilica Dual-Layer Hollow Fibers with Enhanced Selectivity and Flux as Novel Membranes for Ethanol Recovery

Panu Sukitpaneenit and Tai-Shung Chung*

Department of Chemical & Biomolecular Engineering, National University of Singapore, 10 Kent Ridge Crescent, 4 Engineering Drive 4, Singapore 117576, Singapore

 Supporting Information

ABSTRACT: In this work, we have demonstrated the design and engineering of poly(vinylidene fluoride) (PVDF)/nanosilica dual-layer hollow fibers as novel pervaporation membranes for ethanol recovery. The newly developed dual-layer hollow fiber membrane can exhibit a high separation factor of up to 29 with a sustainable high flux of $1.1 \text{ kg m}^{-2} \text{ h}^{-1}$, which is equivalent to the separation performance regime of inorganic membranes. Central to this performance achievement is the synergy of (1) desirable membrane morphology, nanopore size, and high surface porosity of a thin-PVDF/nanosilica composite on a fully porous substrate accomplished by the dual-layer coextrusion technology, and (2) optimal operating downstream pressure with the aid of controlled pervaporation transport. The membrane selectivity-downstream pressure dependence of PVDF/nanosilica hybrid membranes is comprehensible via a modified pore-flow model. This study may represent a new class of membranes for ethanol–water separation.

1. INTRODUCTION

The world is advancing toward a new era where energy demand is constantly burgeoning, because of the rapid growth in population and industrialization, coupled with the depletion of conventional fossil fuels, the escalation in oil prices, and the increasing severity of global warming and climate changes. Subsequently, energy crisis and environmental protection have become major global concerns, and much interest has been placed in developing alternative energy sources that are renewable, viable, and environmentally friendly. Biofuel such as bioethanol represents one of the most successful renewable and sustainable fuels alternatives to fossil fuels. In recent years, many countries worldwide have initiated extensive research and legislative programs to exploit biofuel, primarily bioethanol in a broad scale.^{1–3} Bioethanol today constitutes ~15% of the entire U.S. gasoline consumption, and its market share is predicted to reach 53% of the U.S. gasoline demand in 2030.⁴

To date, commercial bioethanol is typically produced from the fermentation of corn and sugar-based feedstocks. This leads to controversial issues regarding the competitive usage of land and price of these food crop feedstocks with agricultural aspects. Recently, cellulosic ethanol, derived from lignocellulosic-based biomass, has emerged to address the above-mentioned issues concerning starch-based foods.^{5,6} This next-generation biofuel is expected to play a promising role in sustainable development. Hence, there is a great interest in developing a cost-effective technology for extracting ethanol derived from nonfood lignocellulosic feedstocks.

One of the challenges faced by such feedstocks is that lignocellulose-based fermentations typically produce a more dilute concentration of ethanol than that from corn- or sugar-cane-based fermentations:^{7,8} 1–6 wt % from lignocellulosic feedstocks, but 8–15 wt % from starch-based feedstocks. The low concentration of ethanol poses a problem for conventional distillation processes; distillation energy requirements (and cost)

increase exponentially at low ethanol feed concentrations.^{9,10} Furthermore, questions concerning the net environmental impact of bioethanol purified by distillation have been raised.¹¹ A more efficient and greener separation process is pursued to significantly reduce the energy footprint of bioethanol production from lignocellulosic feedstocks, and even for starch-based feedstocks. This circumstance signifies a clear view that alongside tremendous efforts devoted to the advancements in biosciences and bioengineering on the design and engineering of the genetic transformation of biomass into biofuel,¹² a major breakthrough in the separation and purification of biofuel from fermentation products is of paramount importance.

Pervaporation is a membrane-based separation process that has the potential to provide an energy- and cost-effective alternative to a traditional distillation for the recovery of alcohols from fermentation broths.^{11,13–15} In pervaporation, the liquid containing dilute ethanol is brought into contact with one side of the membrane while a vacuum or gas purge is applied on the other side to produce a permeate vapor on the other side of the membrane.¹⁶ In a recent review on various separation technologies for alcohols recovery by L.M. Vane,¹⁰ pervaporation could be a promising choice to compete with a standard distillation, in terms of energy efficiency, in particular, for a cellulosic ethanol process in which the ethanol content in broths is relatively low. In addition, the unique advantage of pervaporation includes the potential to be integrated with the existing processes.^{17–19} In a recent work by Ding et al.,²⁰ integrating membrane pervaporation with a fermentor resulted in the improvement of ethanol productivity. Besides the above-mentioned benefits, other attractive

Received: September 15, 2011

Accepted: December 9, 2011

Revised: December 1, 2011

Published: December 09, 2011

features of pervaporation include minimum contamination, compact operation unit space, and environmental friendliness.

Despite its apparent economic and environmental advantages and great application potential, the absence of desirable membrane materials that combine a high selectivity—high flux separation characteristic with a cost-effective fabrication is a significant obstacle hindering further advancement of this technology in the industrial practice. Vane's evaluation of the energy efficiency of pervaporation to replace a current standard distillation suggested that membranes with an ethanol–water separation factor of >20 are necessary in order to achieve its energy-saving proficiency.^{10,21}

To date, several membrane materials ranging from polymeric, inorganic and composite (mixed-matrix) materials have been extensively investigated but have yet received a breakthrough in the development. Poly(dimethylsiloxane) (PDMS) or well-known as “silicone rubber” is a benchmark material and the most widely studied for ethanol recovery. Tremendous effort has been given to enhance the ethanol–water separation factor of PDMS via chemical modifications such as grafting and cross-linking with other materials. However, only a marginal improvement in the separation performance has been achieved with a significant loss in the total flux. Other polymeric materials, such as polyimide,¹⁴ poly[1-(trimethylsilyl)-1-propyne] (PTMSP),^{22–24} styrene-fluoroalkyl acrylate graft copolymer,²⁵ polyorganophosphazene,²⁶ polyurethaneurea,²⁷ polyether block amide,²⁸ styrene-butadiene-styrene block copolymers²⁹ have also been investigated. Most of the membranes show a trade-off relationship in the separation performance; they possess either an improved separation factor with a significantly reduced flux or an enhanced flux with a lack of selectivity.

Inorganic membranes based on silicalite-1 and hydrophobic zeolites typically exhibit a greater ethanol/water separation factor and flux, relative to polymeric membranes. However, zeolite and silicalite-1 membranes are more difficult and costly to fabricate than polymeric membranes. The idea of incorporating zeolite/silicalite-1 into the polymer matrix, therefore, is of great recent interest, because it combines the benefits of both materials; the exceptional high separation properties and thermal resistance of silicalite-1/zeolites with the desirable mechanical integrity, the low price, and ease of membrane fabrication of polymers.^{30,31} The incorporation of silicalite-1 or hydrophobic zeolites into PDMS polymer matrix have been intensively studied.^{32–35} Besides mixed-matrix membranes based silicalite-1 or zeolite, new hybrid or composite membranes containing other different fillers, such as polyphosphazene nanotubes,³⁶ carbon black,³⁷ silica³⁸ have been studied, and their separation performances mostly fall between PDMS and silicalite-1/PDMS membranes. At present, PDMS and silicalite-1/PDMS composite membranes have been manufactured by many companies such as Sulzer Chemtech (Neunkirchen, Germany), SolSep BV (Apeldoorn, Netherlands), Pervatech BV (Enter, The Netherlands).³⁹ However, the limited efficacy in a high selectivity with an elevated flux and membrane stability of available membrane materials has yet to compete with distillation for ethanol recovery. Without the development of an appropriate membrane, pervaporation is unlikely to materialize as a viable alternative ethanol recovery technique.

Recently, the potential of PVDF membranes as alternative membrane materials for ethanol–water separation has been explored.⁴⁰ The key advantages of PVDF over most conventional polymers such as PDMS include its highly hydrophobic nature, good mechanical property, and excellent chemical resistance, which are vital requirements for pervaporation membranes as

they come into contact with liquid mixtures. In addition, its hollow fiber configuration offers many advantages, such as a higher permeation flow per unit volume, self-contained vacuum channel on the lumen side, and ease of handling during module fabrication and system operation. Compared with polymeric membranes available in the literature, the PVDF hollow fibers exhibited a remarkable high flux of 3.5–8.8 kg m⁻² h⁻¹ and reasonable ethanol–water separation factor up to 8. However, as mentioned earlier, the membrane selectivity must be improved at least up to separation factor of 20 to meet its potential applications.

The success of membrane development is not only relied on the advancements in membrane materials and fabrication techniques but also requires a proper understanding in the mass transport across the membrane. Our previous studies^{40,41} have proved that the pervaporation transport in PVDF hollow fiber membranes for ethanol/water separation can be satisfactorily described via a modified pore-flow concept, rather than a solution-diffusion model, which is widely employed in the majority of the studies. Hence, this leads to different strategies in developing membrane structure and operating conditions. For example, in the solution-diffusion approach, the ideal membranes are dense and a thin selective layer is therefore required to maximize the membrane selectivity and flux, respectively.^{42,43} Conversely, the membranes following the modified pore-flow model have a relatively porous structure whereby the pore size, surface porosity, and hydrophobicity play a crucial role in determining the separation performance. In fact, a thin hydrophobic porous selective skin composing fine pores and high surface porosity is the preferential membrane structure for the modified pore-flow concept. Recent studies have proven that the incorporation of finely dispersed organic and inorganic particles, i.e., organophilic clay,^{44,45} polytetrafluoroethylene (PTFE) (Teflon),⁴⁶ SiO₂,^{47–49} TiO₂,^{50,51} Al₂O₃,⁵² and ZrO₂⁵³ in the PVDF polymer matrix is a very useful approach in altering the membrane surface properties. For instance, adding silica into the PVDF polymer matrix possibly resulted in the formation of fine pore size, high porosity, strong membranes, as well as the alteration of membrane surface hydrophobicity. Meanwhile, the advanced fabrication of hollow fibers by means of the coextrusion technology can help to accomplish a relative thin selective porous skin in addition to the benefit of saving material cost.^{44,54,55}

Besides the different approaches in designing a favorable membrane structure, the identification of appropriate operating conditions for each type of membranes is also important in particular the role of downstream pressure. In the last 30 years, only very limited publications have been given to discuss the significance of downstream pressure on pervaporation,^{56–60} but most of them were based on dense membranes with the solution-diffusion mechanism approach. Typically, the downstream pressure is suggested to be kept as low as possible (most-often reported under vacuum conditions of 0–100 Pa) in order to create the maximum driving force of mass transport across the membrane.⁵⁷ This practice has been widely adopted to conduct experiments in academic research, despite the fact that it would be more reasonable and cost-effective to examine the pervaporation process at relatively higher downstream pressures (up to several thousand pascals), because of the technical difficulty of achieving and keeping relatively low vacuum in the industrial practical scale.⁵⁹ However, the same practice may not be appropriate for the pore-flow membranes, where the pressure gradient may significantly interfere the mass transport in the selective pore

which involves the evaporation/liquid–vapor phase change. It would be worthwhile to investigate and understand the influence of downstream pressure from the modified pore-flow model, which has yet to be reported in the literature.

Therefore, the objective of this work is to design PVDF/nanosilica dual-layer hollow fiber membranes molecularly with an enhanced selectivity (ethanol–water separation factor up to 29) and a high total flux for ethanol recovery via tuning membrane morphology and controlling the operating downstream pressure employing the modified pore-flow concept. The desirable membranes should have the following characteristics: (1) a relative thin PVDF/nanosilica composite outer layer; (2) a highly porous and sponge-like inner layer; and (3) delamination-free at the interface. In this regard, the incorporation of hydrophobic silica nanoparticles and optimization of spinning parameters such as air gap, take-up speed, and outer-dope flow rate were studied. A relationship among corresponding membrane morphology, pore size, porosity, hydrophobicity, and separation performance was elaborated. The significance of downstream pressure on membrane separation and pervaporation mass transport was investigated, and the modified pore-flow model was further employed to predict and understand such separation–downstream pressure-dependent phenomenon. A comparison of the separation performance of developed hollow fiber membranes with various membranes available in the literature was highlighted. To our best knowledge, this work not only establishes the development of high-performance pervaporation membranes for ethanol recovery, but also provides the fundamental science and understanding of tunable pervaporation characteristics from the aspects of membrane morphological design and downstream pressure control.

2. EXPERIMENTAL SECTION

2.1. Materials. Poly(vinylidene fluoride) (PVDF), Kynar HSV 900 was purchased from Arkema, Inc. Hydrophobic silica, AEROSIL R 972 (average particle size = 16 nm; specific surface area (BET) = $110 \pm 20 \text{ m}^2 \text{ g}^{-1}$; tapped density $\approx 0.50 \text{ g L}^{-1}$, SiO₂ content $\geq 99.8 \text{ wt } \%$, spherical shape with free of pores) was provided by Evonik Degussa Chemicals (Germany). Its high hydrophobicity (water contact angle $\approx 105^\circ$)⁶¹ is attributed to the surface modification with Dimethylidichlorosilane (DDS). PVDF and silica were dried overnight under vacuum 60 °C prior to use. N-methyl-2-pyrrolidone (NMP) from Merck was used as the solvent for dope preparation. Analytical-grade ethanol from Merck and distilled water were utilized to conduct the pervaporation tests. All reagents were used as received.

2.2. Dope Preparation and Dual-Layer Hollow Fiber Fabrication. The homogeneous PVDF/NMP dope solution was prepared according to the procedure reported elsewhere;⁶² PVDF powder was dissolved in NMP, and the polymer solution was then subsequently stirred at 60 °C for 24 h to ensure complete dissolution of the polymer. For the heterogeneous PVDF/NMP dope containing silica, a slight modification on the dope preparation was made as follows; the desired amount of silica nanoparticles was first dispersed into NMP and the mixture was then stirred continuously for 24 h under a high-speed agitation of 400–500 rpm in order to break down particle aggregations and to enhance the dispersion of the particles.⁵⁴ After that, PVDF was slowly added into the dispersed nanosilica/NMP mixture and stirred for 24 h. All the dope solutions were

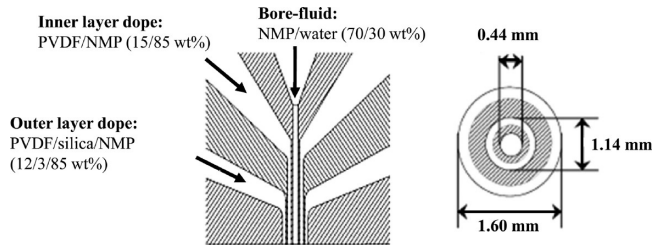


Figure 1. Schematic diagram of spinneret for dual-layer hollow fiber spinning.

degassed in an ultrasonic bath for several hours and then in the ISCO syringe pumps for another 12 h before spinning.

The PVDF/NMP dope solutions with and without silica were employed as outer layer and inner layer membrane materials, respectively in the fabrication of PVDF/silica dual-layer hollow fiber membranes using a dry-jet wet spinning process via the coextrusion of polymer dopes through a dual-layer spinneret. A detailed description of the hollow fiber spinning process is documented elsewhere.^{62,63} Figure 1 depicts a schematic of the dual-layer spinneret and its dimension used in this study. Table 1 lists the sample identification, dope compositions, and spinning conditions of hollow fiber membranes with various air-gap lengths, take-up speeds, and outer-dope flow rates. The dope with 20 wt % silica loading (i.e., the weight ratio of silica to the sum of silica and PVDF polymer) was deliberately chosen in this work, due to the composition being able to accommodate the highest silica loading while preserving the appropriate dope viscosity (spinnability) simultaneously. From our experimental observation, the dope prepared with a higher silica loading (>20%) exhibited an excessively high viscosity, an inhomogeneous solution, and a difficulty for spinning at room temperature. The spinning conditions at an elevated air gap of 20 cm and high take-up speed of 7 m min⁻¹ were adopted from our previous study to facilitate the suppression of macrovoids and large defects/pore formation during membrane precipitation.⁴⁰ Other spinning parameters were kept constant throughout the spinning process. The as-spun hollow fibers were immersed in water for at least 3 days to ensure thorough removal of residual NMP solvent. Subsequently, the hollow fibers were freeze-dried for 24 h before further characterization.

2.3. Membrane Characterization. The morphology of dual-layer hollow fiber membranes was observed using scanning electron microscopy (SEM) (JEOL, Model JSM-5600LV) and field-emission scanning electron microscopy (FESEM) (JEOL, JSM-6700LV). The dispersion of silica in the outer layer matrix was examined using X-ray energy-dispersive spectrometry (EDX) (Oxford INCA equipped with the JEOL JSM-5600LV SEM system) elemental mapping technique. The contact angle of hollow fiber membranes was measured using a KSV Sigma 701 Tensiometer (KSV Instruments Ltd., Finland) at 25 °C. The overall porosity was determined using a gravimetric method (kerosene is a wetting liquid). The detailed specimen preparation and procedures for the contact angle and overall porosity measurement have been described in our previous study.⁴⁰

The mean pore size and effective surface porosity of hollow fiber membranes were characterized using the gas permeation method. The experimental apparatus and procedures for hollow fiber design have been described elsewhere.⁴¹ Each module consists of two fibers with an effective length of ~5 cm. Pure

Table 1. Spinning Conditions and Parameters of PVDF/Nanosilica Dual-Layer Hollow Fiber Membranes with a Thin Composite Outer Layer

spinning code	Parameter ^a				
	outer-layer dope composition (wt%)	inner-layer dope composition (wt%)	outer-layer dope flow rate (cm ³ min ⁻¹)	air-gap distance (cm)	take-up speed (m min ⁻¹)
Effect of Air-Gap Distance					
DL _{AG-20}	PVDF/nanosilica/NMP 12/3/85	PVDF/NMP 15/85	0.2	20	free flow
Effect of Take-up Speed					
DL _{TK-7}	PVDF/nanosilica/NMP 12/3/85	PVDF/NMP 15/85	0.2	1	7
Effect of Outer-Dope Flow Rate					
DL _{AG-20-ODR-0.1}	PVDF/nanosilica/NMP 12/3/85	PVDF/NMP 15/85	0.1	20	free flow
DL _{AG-20-ODR-0.4}	PVDF/nanosilica/NMP 12/3/85	PVDF/NMP 15/85	0.4	20	free flow

^a Inner-dope flow rate = 2.0 cm³ min⁻¹; bore-fluid composition = 70/30 wt % water/NMP; bore-fluid flow rate = 0.6 cm³ min⁻¹; external coagulant = tap water; coagulant bath and spinning temperature = 25 °C; relative humidity = 65%.

nitrogen was used as the test gas. The gas permeation rate was measured using a soap-bubble flow meter at various transmembrane pressure differences from 0 to 103.42 kPa at room temperature. The gas permeance (G) was determined using the following equation:

$$G = \frac{F}{A_a \Delta P} = \frac{F}{n\pi D l \Delta P} \quad (1)$$

where G is the gas permeance (mol m⁻² Pa⁻¹ s⁻¹), F the total gas permeation rate (mol s⁻¹), A_a the effective membrane area (m²), n the number of fibers in one testing module, D the outer diameter of the hollow fiber (cm), l the effective length of the modules (cm), and ΔP the gas pressure difference across the membrane (Pa).

In a porous asymmetric hollow fiber membrane, the gas transport mechanism can be considered as the combination of Knudsen flow and Poiseuille flow.^{64,65} By assuming cylindrical pores in the selective skin layer, the total gas permeance can be calculated as follows:

$$G = \frac{2}{3} \left(\frac{8RT}{\pi M} \right)^{1/2} \frac{1}{RT} \left(\frac{r \varepsilon_s}{\delta} \right) + \frac{P_m}{8\eta_g RT} \left(\frac{r^2 \varepsilon_s}{\delta} \right) \quad (2)$$

or rewritten as

$$G = I_0 + S_0 P_m \quad (3)$$

where r is the mean pore size of the membrane (m), ε_s the surface porosity, δ the effective pore length (m), η_g the gas viscosity (Pa s), R the gas constant (8.314 m³ Pa mol⁻¹ K⁻¹), P_m the mean pressure (Pa), M the molecular weight of the gas (kg mol⁻¹), and T the absolute temperature (K).

By plotting G against mean pressures according to eq 3, the mean pore size and effective surface porosity over pore length (ε_s/δ) can be calculated from the intercept (I_0) and slope (S_0) as follows:

$$r = \frac{16}{3} \left(\frac{S_0}{I_0} \right) \left(\frac{8RT}{\pi M} \right)^{1/2} \eta_g \quad (4)$$

$$\frac{\varepsilon_s}{\delta} = \frac{8\eta_g R T S_0}{r^2} \quad (5)$$

There is a significant distinction between the term "effective surface porosity", which is defined as ε_s/δ in eq 5, and the term

"surface porosity, ε_s ". The former has units of m⁻¹, while the latter has no units.

2.4. Membrane Module Fabrication and Pervaporation Tests.

Two pieces of fibers were assembled into the module holder, which consists of two Swagelok stainless steel male runtees connected by a PFA tube. Both ends of the module were sealed with a slow cure epoxy resin (KS Bond EP231, Bondtec). The modules were mounted onto the pervaporation setup with the shell side in contact with the feed solution and an effective length of the fiber of ~15 cm. The detailed design and operating procedures of the equipment for the hollow fiber membrane pervaporation have been documented elsewhere.^{40,60,66} A minimum of three modules with the same fabrication condition were examined for each pervaporation condition. Two liters (2 L) of a 5 wt % ethanol/water mixture with a recirculation rate of 30 L h⁻¹ was used as the feed solution. The operating temperature was maintained at 50 °C throughout the experiment. The upstream pressure was at atmospheric pressure (101.325 kPa), while the downstream pressure was controlled by a vacuum pump (Edward RVS, USA). The total permeate (downstream) pressure was regulated by introducing bleed air via an adjustable valve and the pressure was measured using a Digital Vacuum Regulator (Vacuubrand, USA), both are located between the cold trap and the vacuum pump. The system was stabilized for 1 h before the collection of samples to account for system dynamics. According to the observation in this study, 1 h was sufficient for both the permeate flux and composition to reach a stable state. The permeate vapor was condensed in a cold trap, which was immersed in liquid nitrogen.

In our experiments, the downstream pressure is varied from a low pressure to a high pressure. There was no liquid observed in the permeate side as long as the downstream pressure was kept below the saturated vapor pressure. When the downstream pressure was increased to a certain value (close to and above saturated vapor pressure), the presence of condensed liquid in the permeate line was clearly observed. To avoid the misleading results from this phenomenon due to the fact that some accumulated permeates could possibly not reach the cold trap, the condensed permeates were collected for analyses by applying a full vacuum (with turning off the valve near the module) for a very short time (<1 min) to suck all condensed permeate from the tube to the cold trap. Since the time applied for this practice is short, the effect of membrane swelling under untreated vacuum can be neglected.⁶⁸ The same practice had been adopted from the literature.

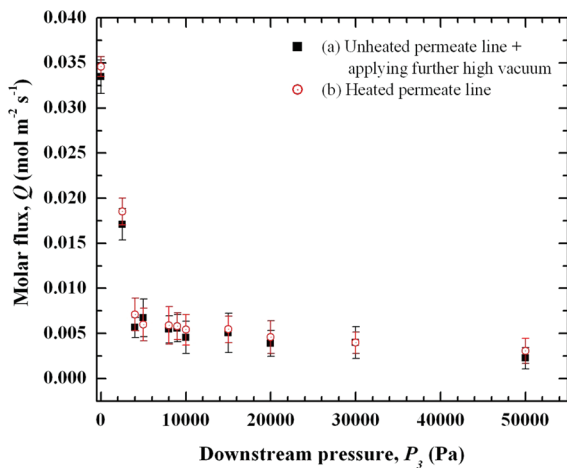


Figure 2. A comparison of experimental data on pervaporation of pure water system as a function of downstream pressures using different permeate collecting approaches: (■) unheated permeate line with partial condensates in the permeate line, which was further recovered by applying a high vacuum and (○) heated permeate line at 35 °C with no condensation observed along the permeate line.

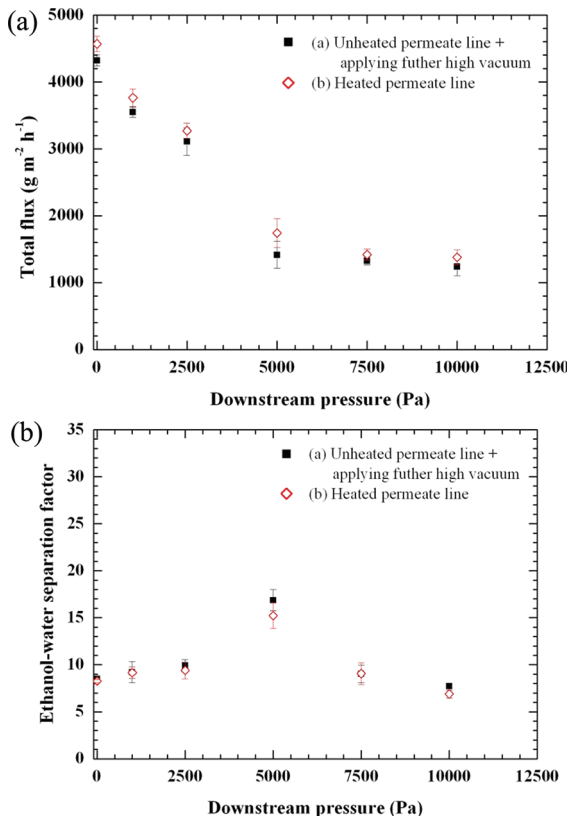


Figure 3. Pervaporation performance in terms of (a) total flux and (b) separation factor at various downstream pressures in a comparison of two different permeate collecting methods: (■) unheated permeate line with partial condensates in the permeate line, which was further recovered completely by applying a high vacuum, and (○) heated permeate line at 35 °C with no condensation observed along the permeate line. (The feed solution is 5 ± 0.5 wt % ethanol/water; the feed temperature is 50 °C; and the membrane spinning code DL_{AG-20} is used.)

In this circumstance, one may be concerned with whether this collection method is sufficient to provide reasonable and reliable

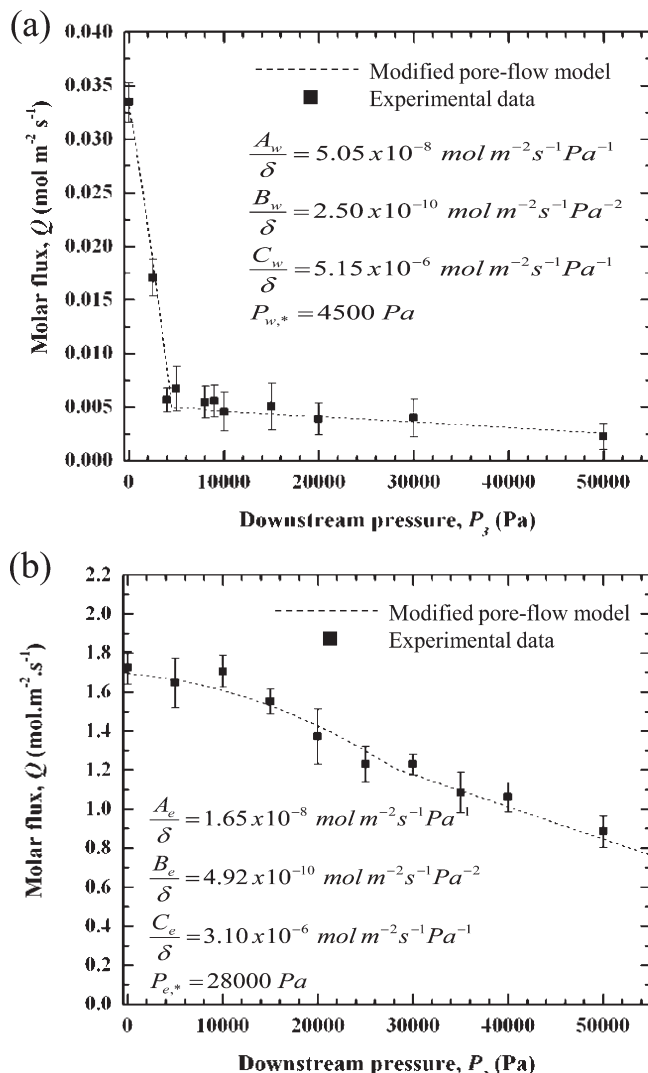


Figure 4. Estimation of transport parameters in the modified pore-flow model from the pervaporation data of pure-component systems at 50 °C: (a) pure water and (b) pure ethanol (spinning code: DL_{AG-20}).

results. Hence, we have carried out additional experiments by using heated permeate lines, to investigate the significance of condensation in our pervaporation tests. In this study, the permeate line was wrapped with flexible insulated heating tapes. The temperature of the line was regulated using a temperature controller. In this experiment, the permeate line temperature was set and maintained at 35 ± 1 °C. The temperature was chosen as an optimal condition for the heat up of the permeate line with the following considerations: (1) based on our experimental setup and careful observations, this moderate temperature is sufficient enough to prevent condensation; (2) it is more convenient to maintain the condition with a low temperature variation throughout the testing; and (3) a higher temperature may complicate the case as the temperature gradient may affect and cause unexpected results. Another pressure gauge was placed between the membrane module and cold trap to monitor the pressure drop along the vacuum line. From our observations, the relative pressure drop is <5 mbar (compared with the one located between a cold trap and vacuum pump) in all testing conditions. The pervaporation was carried out in both pure water and 5 wt % ethanol/water

as feed solutions, and the same membrane DL_{AG-20} was used. The results are presented in Figures 2 and 3, respectively.

Based on the results, it can be seen that there is no significant difference of the membrane flux (and separation factor) in both permeate collection methods as most data points are comparable within a region of experimental errors. In our previous testing method, although the condensation can be observed at the higher downstream pressures, only a small ratio of liquid condensates to the total collected permeate at the cold trap (<5 wt %) was occurred. In addition, in our pervaporation system design, the cold trap was placed at a lower height, relative to the membrane module, which may help to prevent the condensate accumulation along the tubing and meanwhile facilitate the condensate recovery once the high vacuum is applied. Therefore, based on the results and our careful observations during the experiments, applying a high vacuum is found to be sufficient and effective in this study to account for the contribution of condensation in addition to the heated permeate line technique.

The sample was collected at 1-h intervals for 4 h and weighed by a Mettler Toledo balance. The sample compositions were analyzed with three parallel injections by a Hewlett-Packard Model GC 6890 with a HP-INNOWAX column (packed with cross-linked polyethylene glycol) and a TCD detector. The feed content varied by <1 wt % during the entire experiment and, therefore, can be considered to be constant, because of the large quantity of feed solution, in comparison with the permeate sample. The total flux (W_{total}) ($\text{g m}^{-2} \text{ h}^{-1}$) and separation factor ($\alpha_{\text{ethanol/water}}$) were calculated using the following equations:

$$W_{\text{total}} = \frac{J}{A_a t} \quad (6)$$

$$\alpha_{\text{ethanol/water}} = \frac{Y_e / Y_w}{X_e / X_w} \quad (7)$$

$$Y_{w,3} = \frac{\frac{B_w}{\delta}(P_{w,*}^2 - P_{w,3}^2) + \frac{C_w}{\delta}(P_{w,*} - P_{w,3})}{\frac{B_w}{\delta}(P_{w,*}^2 - P_{w,3}^2) + \frac{C_w}{\delta}(P_{w,*} - P_{w,3}) + \frac{B_e}{\delta}(P_{e,*}^2 - P_{e,3}^2) + \frac{C_e}{\delta}(P_{e,*} - P_{e,3})} \quad (11)$$

To be expressed in terms of downstream pressure (P_3), eq 11 can be rewritten as

$$Y_{w,3} = \frac{\frac{B_w}{\delta}[P_{w,*}^2 - (P_3 Y_{w,3})^2] + \frac{C_w}{\delta}[P_{w,*} - (P_3 Y_{w,3})]}{\frac{B_w}{\delta}[P_{w,*}^2 - (P_3 Y_{w,3})^2] + \frac{C_w}{\delta}[P_{w,*} - (P_3 Y_{w,3})] + \frac{B_e}{\delta}[P_{e,*}^2 - (P_3(1 - Y_{w,3}))^2] + \frac{C_e}{\delta}[P_{e,*} - (P_3(1 - Y_{w,3}))]} \quad (12)$$

where $Y_{w,3}$ is the water mole fraction in the permeate side, and B_w/δ and B_e/δ ($\text{mol m}^{-2} \text{ s}^{-1} \text{ Pa}^{-2}$) are the vapor transport coefficients contributed by the surface flow of water and ethanol components, respectively. C_w/δ and C_e/δ ($\text{mol m}^{-2} \text{ s}^{-1} \text{ Pa}^{-1}$) are the vapor transport coefficients contributed by the Knudsen flow of water and ethanol components, respectively. $P_{w,*}$ and $P_{e,*}$ (Pa) are the partial vapor pressures of the water and ethanol components in the saturated vapor, respectively.

From eq 12, the permeate water mole fraction ($Y_{w,3}$) under various downstream pressures can be calculated using the

where J is the total mass (g) transferred over time t (h), and A_a is the effective membrane area (m^2). X_e and Y_e are the mole fractions of ethanol in the feed and permeate, respectively, and X_w and Y_w are the mole fractions of water in the feed and permeate, respectively.

2.5. Modified Pore-Flow Model for Pervaporation Transport Analyses. The modified-pore flow model was proposed in our previous study⁴¹ and was established based on the assumptions that there are a bundle of straight cylindrical pores penetrating across the selective layer of the membranes and that all the pores are operating under an isothermal condition. The mass transport in the pore can be considered as a combination of liquid-phase and vapor-phase transport in series where the vapor transport is governed by surface flow and Knudsen flow mechanisms. According to the model, the mass transport, in terms of total molar flux of a pure component system, can be represented as

$$Q_{\text{total}} = Q_{\text{liquid}} + Q_{\text{surface}} + Q_{\text{Knudsen}} \quad (8)$$

$$Q_{\text{total}} = \frac{A}{\delta}(P_2 - P_*) + \frac{B}{\delta}(P_*^2 - P_3^2) + \frac{C}{\delta}(P_* - P_3) \quad \text{when } P_3 < P_* \quad (9)$$

$$Q_{\text{total}} = \frac{A}{\delta}(P_2 - P_3) \quad \text{when } P_3 \geq P_* \quad (10)$$

Details on the theoretical background and equation derivations have been documented in our previous study.⁴¹ Definitions of the symbols are given in the Nomenclature section.

The prediction of the mole fraction of water at the permeate side in a binary system using the transport parameters from pure component systems can be obtained using the following equation:

mathematics computation (MATLAB computing software), whereby all transport parameters and saturation vapor pressures for respective pure component systems can be attained by fitting the experimental data to eqs 9 and 10. Figure 4 illustrates a typical pattern of curve characteristics in the pervaporation of pure water (Figure 4a) and pure ethanol (Figure 4b) systems for hollow fiber membranes spun with a 20 cm air gap (DL_{AG-20}). All membranes exhibited a similar curve pattern but differed in values of the transport parameters and saturation vapor pressures.

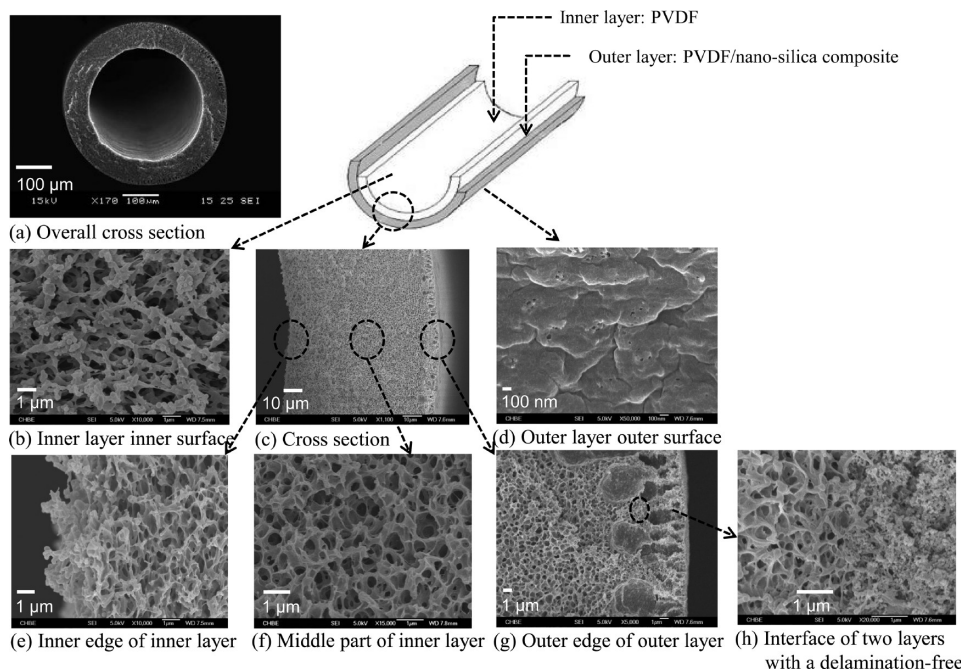


Figure 5. SEM and FESEM images of different bulk and surface morphologies of PVDF/nanosilica composite dual-layer hollow-fiber membranes (spinning code: DL_{AG-20}).

3. RESULTS AND DISCUSSION

3.1. Membrane Characterizations. A typical morphology of PVDF/nanosilica dual-layer hollow-fiber membranes spun with an air gap of 20 cm (DL_{AG-20}) is shown in Figure 5. The cross-sectional morphology reveals that the membrane consists of a fully porous PVDF inner layer, a relatively thin PVDF/nanosilica composite outer layer, and a delamination-free interface. The surface and bulk morphologies of the inner layer of the hollow fiber has a highly porous structure, which is desirable for minimizing the substructure resistance.⁴⁰ The outer surface of the outer layer, which is composed of the PVDF/nanosilica composite (Figure 5d), is relatively dense and seemingly comprised of tiny voids formed at the nodular edge and the surrounding area of dispersed silica particles. Upon closer scrutiny, the enlarged cross-sectional morphology (Figure 5g) depicts very small pores beneath the outer layer surface. With the consideration of these voids or defects as pores on the membrane surface, the developed membrane structural feature is identical with the conceptual structure in the modified pore-flow concept. Similar bulk and surface morphologies as discussed above are obtained for the hollow fibers spun with other conditions.

The distribution of filler particles in the polymer matrix is another major concern in fabricating the nanocomposite or mixed-matrix membranes. In this study, the distribution of nanosilica in the dual-layer hollow-fiber membrane morphology was monitored by EDX-SEM, as shown in Figure 6. A typical silica distribution through the cross section and outer surface morphologies of the hollow-fiber condition DL_{AG-20} is presented in Figure 6a. It can be qualitatively observed that the silica was dispersed thoroughly across the composite layer and the outer surface of the membrane. Figure 6b displays the silica distribution profile in a line-scan mode of hollow fibers spun with different air-gap length, take-up speed, and outer-dope flow rate. A sharp appearance of high silica intensity in the profile not only confirms the existence of nanosilica in the outer layer but also allows us to estimate the thickness of the

composite outer layer. Depending on the spinning conditions, the thickness of composite layer falls in the range of 3–18 μm. The high take-up speed or low outer-dope flow rate results in a reduced composite outer-layer thickness. The EDX result also supports the achievement of membranes consisting of a thin PVDF/nanosilica composite layer bonded on a thick fully porous substructure.

Table 2 tabulates the membrane properties of as-spun PVDF/nanosilica hollow-fiber membranes, which includes the mean pore size, effective surface porosity, overall porosity, and water contact angle. It can be seen that all resultant membranes possess a mean pore size in the range of 50–62 nm, with an effective surface porosity of the magnitude of 10² and an overall bulk porosity of ~69%. Such pore characteristics may be attributed to the combination effect of (1) the incorporation of nanosilica into the PVDF matrix, which could help in achieving a small pore size with a high surface porosity,⁴⁸ and (2) the elongation stress via spinning at a high air gap or high take-up speed, which has been discussed in our previous studies.⁴⁰ Additional evidence can be drawn from the fact that the membranes with a thinner composite outer-layer thickness resulting from the higher elongation stress (i.e., DL_{TK-7} and DL_{AG-20-ODR-0.1}) have a tendency to have a smaller mean pore size with a higher effective surface porosity, compared to membranes having a thicker outer-layer thickness, i.e., DL_{AG-20} and DL_{AG-20-ODR-0.4}.

The hydrophobicity of fabricated hollow fibers with various spinning conditions employed was evaluated by determining the water contact angle at the membrane outer surface. In most cases, membranes show a high water contact angle of 90°–100°, thus reflecting the improvement in the membrane hydrophobicity, compared to the pristine single-layer PVDF hollow fibers (contact angle of 81°–86°). This observation implies that the existence of nanosilica could play an essential role on the enhanced hydrophobicity. It is presumably because of its highly hydrophobic nature (contact angle of 105°), in addition to the significant effect on surface porosity, as mentioned previously.

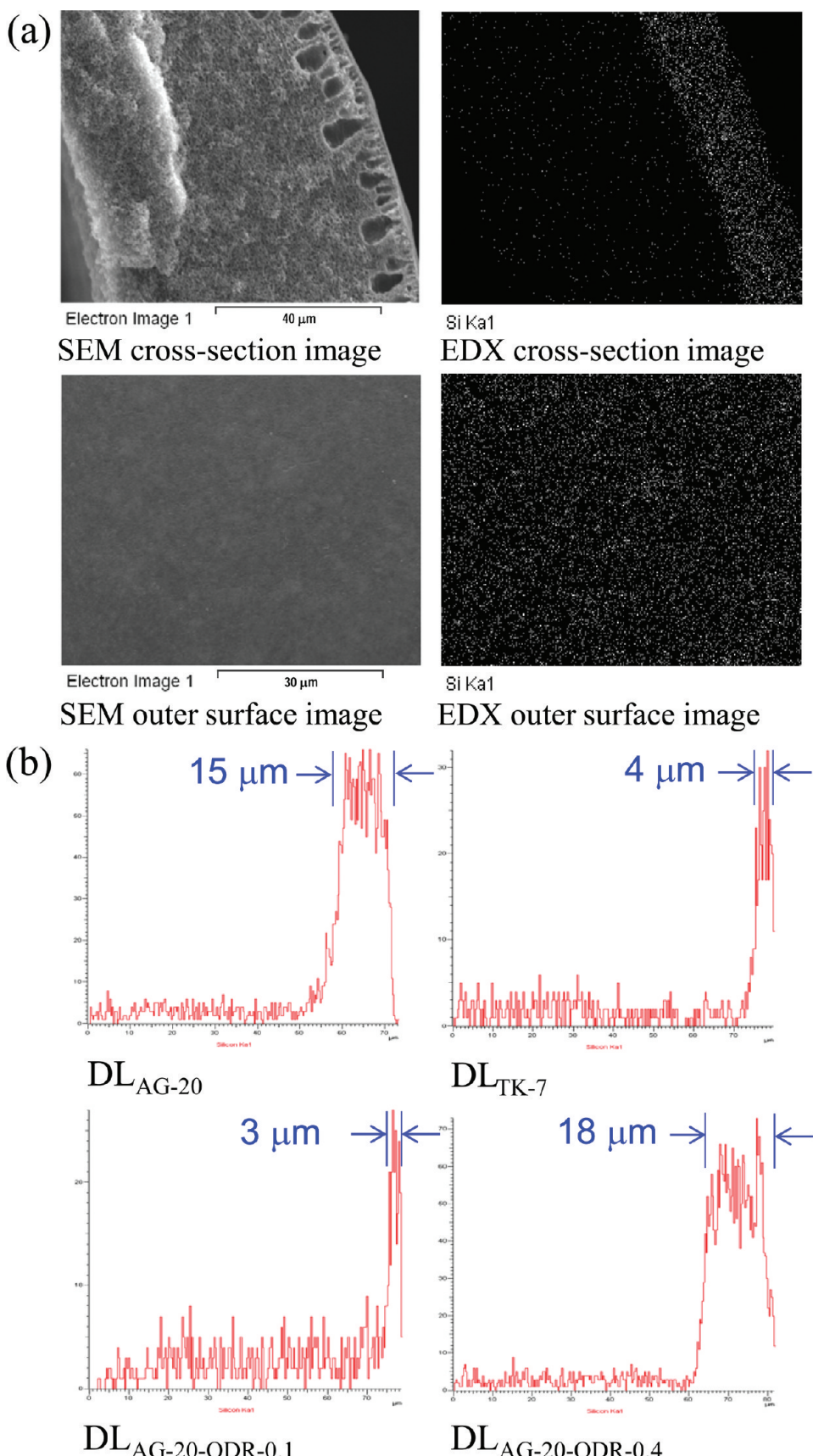


Figure 6. Distribution of silica and the estimation of composite layer thickness of PVDF/nanosilica dual-layer hollow fibers using EDX-SEM characterization: (a) typical silica distribution profile in cross section and outer surface morphologies ($\text{DL}_{\text{AG-20}}$) and (b) the effect of air-gap distance, take-up speed, and outer dope flow rate on the silica distribution profile and the corresponding nanocomposite outer-layer thickness.

Table 2. Membrane Properties of PVDF/Silica Dual-Layer Hollow-Fiber Membranes

membrane	mean pore size, <i>r</i> (nm)	effective surface porosity, ε_s/δ (m^{-1})	overall porosity (%)	water contact angle, θ ($^\circ$)
Effect of Air-Gap Distance				
DL _{AG-20}	62.2 ± 0.6	(6.41 ± 0.62) × 10 ²	68.0 ± 0.5	99.0 ± 2.8
Effect of Take-Up Speed				
DL _{TK-7}	55.0 ± 0.3	(3.94 ± 0.56) × 10 ²	67.0 ± 2.1	88.2 ± 1.8
Effect of Outer-Dope Flow Rate				
DL _{AG-20-ODR-0.1}	50.3 ± 1.2	(8.61 ± 0.18) × 10 ²	68.3 ± 1.3	95.7 ± 3.9
DL _{AG-20-ODR-0.4}	53.1 ± 0.7	(5.83 ± 0.30) × 10 ²	67.4 ± 0.8	96.7 ± 3.1

Table 3. Pervaporation Performance of PVDF/Nanosilica Dual-Layer Hollow-Fiber Membranes under Various Spinning Conditions

spinning code	Permeate Composition (wt%)		Pervaporation Performance ^a		
	ethanol	water	separation factor, $\alpha_{\text{ethanol/water}}$	total flux, W_{total} ($\text{g m}^{-2} \text{ h}^{-1}$)	$\alpha_{\text{ethanol/water}}$ ($\text{g m}^{-2} \text{ h}^{-1}$)
Effect of Air-Gap Distance					
DL _{AG-20}	32.37 ± 0.60	67.63 ± 0.60	8.51 ± 0.23	4321 ± 161	
Effect of Take-Up Speed					
DL _{TK-7}	29.75 ± 0.02	70.25 ± 0.02	7.59 ± 0.01	2639 ± 291	
Effect of Outer-Dope Flow Rate					
DL _{AG-20-ODR-0.1}	31.58 ± 1.0	68.42 ± 1.0	8.61 ± 0.44	4255 ± 269	
DL _{AG-20-ODR-0.4}	31.77 ± 1.0	68.23 ± 1.0	8.74 ± 0.29	4111 ± 387	

^a Feed solution, 5 ± 0.5 wt % ethanol/water mixture; feed flow rate, 30 L h⁻¹; operating temperature, 50 °C; downstream pressure, 0 Pa.

However, note that, for the case of high take-up speed spinning (DL_{TK-7}), a moderate increment of water contact angle is observed, which is possibly due to the lower surface porosity. The same phenomenon has also reported in previous studies.⁴⁰

3.2. Pervaporation Performance of PVDF/Nanosilica Composite Dual-Layer Hollow-Fiber Membranes. The pervaporation tests of PVDF/nanosilica dual-layer hollow fibers spun under different spinning conditions were first carried out using a 5 wt % ethanol feed solution, an operating temperature of 50 °C, and a downstream pressure of ~0 Pa. The corresponding separation performance, in terms of permeation composition, ethanol–water separation factor, and total flux of the membranes, is summarized in Table 3. The membranes spun at a high air-gap length of 20 cm, regardless of different outer-dope flow rates (i.e., DL_{AG-20}, DL_{AG-20-ODR-0.1}, and DL_{AG-20-ODR-0.4}) show a relatively better ethanol–water separation factor, compared to the membrane prepared at a high take-up speed (DL_{TK-7}). This may be attributed to the fact that the DL_{TK-7} membranes possess a lower hydrophobicity, even though their pore sizes are comparable with those of other membranes. The membrane surface porosity has a huge influence on the total flux of the membranes in all cases. Membranes with a higher effective surface porosity/overall porosity have a tendency to produce a greater total permeation flux. The surface porosities presented in Table 2 seem to offer a clearer understanding of its

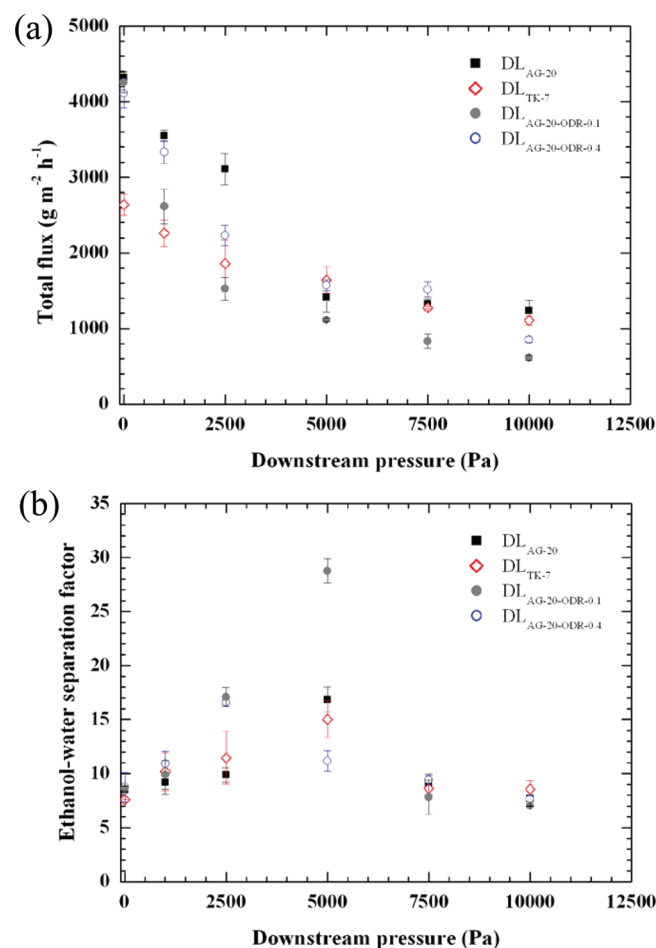


Figure 7. Effect of downstream pressure on pervaporation performance of PVDF/silica nanocomposite dual-layer hollow-fiber membranes with a 5 ± 0.5 wt % ethanol feed solution and at 50 °C: (a) total flux and (b) separation factor.

influence on the flux enhancement, in comparison to the bulk porosities. Overall, all resultant membranes exhibit ethanol–water separation factors of 7.6–8.74 (30–33 wt % ethanol) and total fluxes of 2.6–4.3 kg m⁻² h⁻¹. Despite the fact that the membranes display a remarkably high flux, the membrane selectivity is still lower than our target, which, for at least an ethanol–water separation factor of 20, is preferable to compete with distillation, as stated earlier in the Introduction.

Table 4. Liquid and Vapor Transport Parameters of the Pure-Component System Based on the Modified Pore-Flow Model

membrane	Parameters in Model Equations					
	Pure Water			Pure Ethanol		
Liquid Transport	Vapor Transport		Liquid Transport		Vapor Transport	
A_w/δ ($\text{mol m}^{-2} \text{s}^{-1} \text{Pa}^{-1}$)	B_w/δ ($\text{mol m}^{-2} \text{s}^{-1} \text{Pa}^{-2}$)	C_w/δ ($\text{mol m}^{-2} \text{s}^{-1} \text{Pa}^{-1}$)	saturation vapor pressure, P_{w^*} (Pa)	A_e/δ ($\text{mol m}^{-2} \text{s}^{-1} \text{Pa}^{-1}$)	B_e/δ ($\text{mol m}^{-2} \text{s}^{-1} \text{Pa}^{-2}$)	C_e/δ ($\text{mol m}^{-2} \text{s}^{-1} \text{Pa}^{-1}$)
DL _{AG-20}	5.05×10^{-8}	2.50×10^{-10}	5.15×10^{-6}	4500	1.65×10^{-5}	4.92×10^{-10}
DL _{TK-7}	4.82×10^{-8}	2.05×10^{-10}	4.86×10^{-6}	5000	1.58×10^{-5}	2.25×10^{-10}
DL _{AG-20-ODR-0.1}	4.95×10^{-8}	2.73×10^{-10}	5.90×10^{-6}	4000	1.55×10^{-5}	3.92×10^{-10}
DL _{AG-20-ODR-0.4}	5.25×10^{-8}	1.83×10^{-10}	5.12×10^{-6}	2500	1.67×10^{-5}	4.93×10^{-10}
						3.10×10^{-6}
						28000
						3.26×10^{-6}
						35000
						35000
						25000

Figure 7 illustrates the effect of downstream pressure on pervaporation performance of PVDF/nanosilica dual-layer hollow fibers using 5 wt % ethanol as the feed solution at 50 °C. Interestingly, the alteration of downstream pressure shows a great effect on both flux and separation factor behaviors. With the reference to Figure 7a, the total flux initially decreases considerably and then further declines gradually with an increase in downstream pressure for all cases. The curve characteristic on the flux-downstream pressure dependence is somewhat consistent with the curve pattern in the modified pore-flow model. In addition, the declining pattern of total flux as a function of downstream pressures is found to be different for each membrane, particularly at relatively low downstream pressures, while approaching at a high downstream pressure, the linear relationship with comparable flux values is observed for all membranes.

The significance of downstream pressure on membrane selectivity or separation factor is revealed in Figure 7b. While only a slight difference in the ethanol–water separation factor for all membranes (in a range of 7–9) is found at the downstream pressure of ~0 Pa, the enrichment in the separation factor is clearly observed by the increasing downstream pressure. Interestingly, the membrane selectivity can be achieved with an ethanol–water separation factor as high as 29 at the downstream pressure of 5 kPa for the membrane spun at the 20-cm air gap and the 0.1 outer-dope flow rate (DL_{AG-20-ODR-0.1}). For the membranes with other spinning conditions (DL_{AG-20}, DL_{TK-7}, and DL_{AG-20-ODR-0.4}), the incremental separation factors of 15–18 is observed with the different downstream pressures, namely, 2.5 kPa for DL_{TK-7} and 5 kPa for DL_{AG-20} and DL_{AG-20-ODR-0.4}. Another interesting finding is that when the downstream pressure was applied beyond the optimal pressure, a significant drop in the membrane selectivity is obvious in all membranes with the remaining separation factor of 7–9. Based on our observations during experiments, a further increase in downstream pressure results in a continuous reduction of separation factor, coupled with a serious decrease in total flux.

3.3. The Role of Downstream Pressures on Pervaporation Transport and Its Predictability via the Modified Pore-Flow Model. It is clear that the downstream pressure could play a very crucial role on mass pervaporation transport in PVDF/nanosilica dual-layer hollow-fiber membranes, which turns out to provide a great opportunity to enhance the membrane selectivity. In this study, the modified pore-flow model is employed to further verify and understand the selectivity-downstream pressure dependence phenomenon. Table 4 lists the transport parameters and saturation pressure for all membranes obtained from the pure water and pure ethanol system and used in the model equation. It can be seen that the same magnitude in each of the transport parameters (A/δ , B/δ , and C/δ) is presented for all membranes. However, the liquid transport parameters (A/δ) for pure ethanol (magnitude of 10^{-5}) are greater than those for pure water (magnitude of 10^{-8}), which indicates the high hydrophobic and swelling properties of hollow-fiber membranes.^{4f} This information is consistent with the observation during experiments where the fibers showed no swelling in pure water but exhibited high swelling in pure ethanol. The vapor transport parameter B/δ , which refers to the surface flow mechanism obtained in pure ethanol, is always higher than that in pure water. For vapor transport parameter C/δ , which represents Knudsen diffusion contribution, the opposite trend is observed: the calculated C/δ of pure water is higher than that of pure ethanol. From this finding, it possibly infers that the water may preferentially transport via Knudsen diffusion rather than surface flow,

Table 5. Estimation of Pore Size and Total Saturation Vapor Pressure by the Modified Pore-Flow Model

membrane	pore size (nm) ^c	Pore Size from Transport Parameters (nm) ^{a,b}				total saturation vapor pressure for a binary system, P_* , ethanol–water (Pa)	
		Pure Water		Pure Ethanol			
		calculated from A_w/δ	calculated from C_w/δ	calculated from A_e/δ	calculated from C_e/δ		
DL _{AG-20}	62.2	2.51	52.5	91.2	50.5	4970	
DL _{TK-7}	55.0	3.12	80.6	114	86.4	5600	
DL _{AG-20-ODR-0.1}	50.3	2.14	44.8	76.3	46.7	4620	
DL _{AG-20-ODR-0.4}	53.1	2.68	57.4	96.2	62.7	2950	

^a For A_w/δ and A_e/δ , the pore size is calculated from $r = [(A/\delta)(8\eta M/\rho)(\varepsilon_s/\delta)^{-1}]^{1/2}$; the detailed calculations for water and ethanol systems are given in Appendix A.1. ^b For C_w/δ and C_e/δ , the pore size is calculated from $r = (3/2) \times (C/\delta)[\pi M/(8RT)]^{1/2} \times [RT/(\varepsilon_s/\delta)]$; the detailed calculations for water and ethanol systems are given in Appendix A.2. ^c From the gas permeation test.

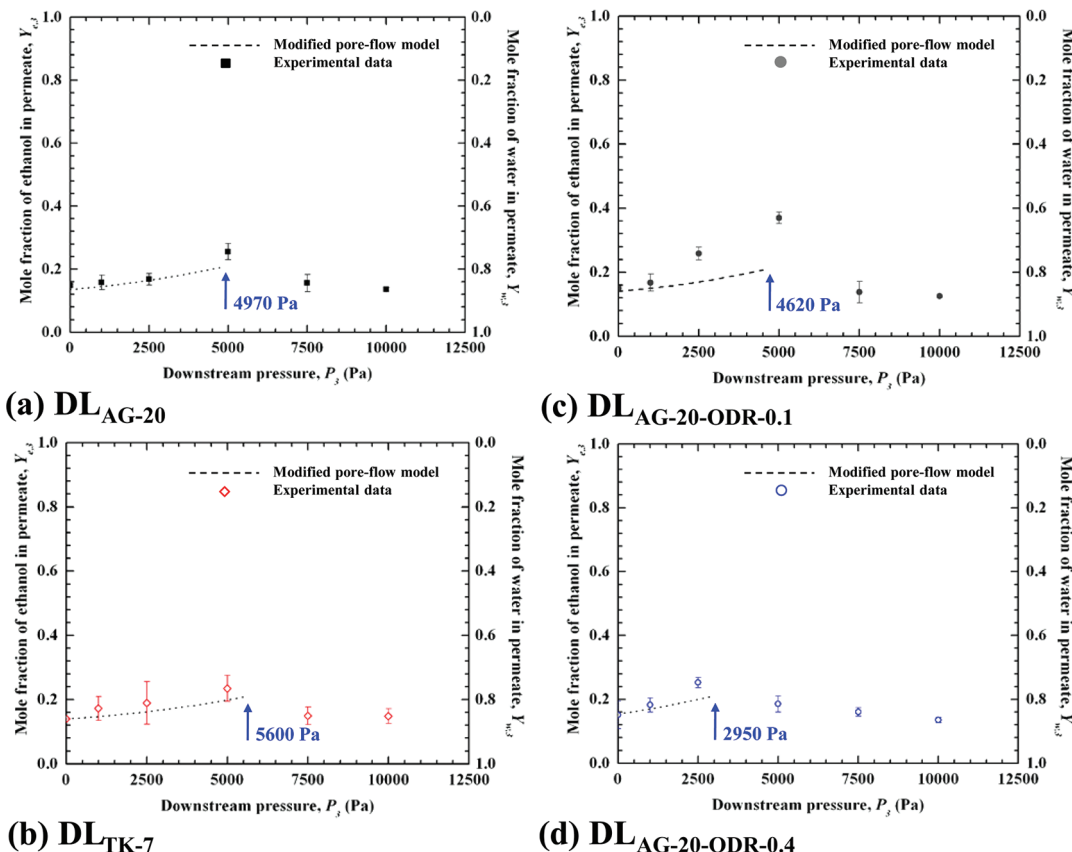


Figure 8. Comparison of ethanol mole fraction at the permeate side as a function of downstream pressures from experiments and theoretical predictions from the modified pore-flow model for various hollow-fiber membranes: (a) DL_{AG-20}, (b) DL_{TK-7}, (c) DL_{AG-20-ODR-0.1}, and (d) DL_{AG-20-ODR-0.4}.

whereas the ethanol may favorably transport via surface flow rather than Knudsen diffusion.

The saturation vapor pressures (P^*) attained for pure water are in range of 2.5–5 kPa for pure water and 28–35 kPa for pure ethanol, which is found to be strongly dependent on each membrane. Compared to the saturation vapor pressure of water (12.4 kPa) and ethanol (29.5 kPa) at 50 °C, as calculated by the Antoine equation,⁶⁷ significant differences in the values can be observed, particularly for the case of water. This can be understood from the fact that, in the pore-flow model, the evaporation phenomenon occurring in the pore can be more complicated especially for cases when the pore is very small, leading

to a strong interaction between the absorbed vapor and the membrane pore. In such a case, the saturation vapor pressure simulated by the pore-flow concept can be different from the literature values.^{68,69} In other words, the saturation vapor pressure of water derived from the modified pore-flow model is lower than that of predicted from a simple evaporation prediction using the Antoine equation most likely due to the nanopore size, great hydrophobicity, and nonswelling property in water of the dual-layer hollow-fiber membranes.

Table 5 summarizes the pore size and total saturation vapor pressure estimated from transport parameters listed in Table 4. It can be observed that the pore size (2.1–3.1 nm) predicted from

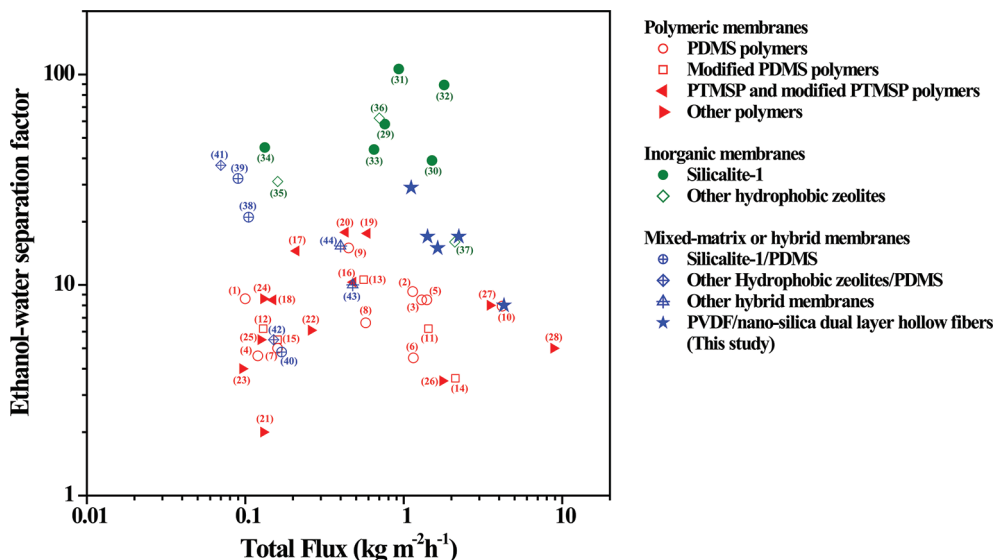


Figure 9. Graphical representation of separation performance of PVDF/nanosilica dual-layer hollow-fiber membranes for ethanol recovery in a comparison with various membranes reported in the literature. Note: The feed ethanol concentration ranges from 3 wt % to 10 wt %; the operating temperature varies from 40 °C to 60 °C.

the liquid transport parameter from pure water tests is smaller than that (50–62 nm) determined from gas permeation tests, whereas the pure ethanol system tests resulted in larger pore size (74–114 nm). The pore size expansion in pure ethanol, compared to that in pure water, may be due to the preferential affinity of ethanol and the strong swelling in the hydrophobic membranes.^{41,70} For both pure-component systems, the pore size predicted from the vapor parameter is similar to that obtained from gas permeation tests. This may be attributed to the similarity in the gas/vapor phase where the strong membrane swelling is compromised, compared to the liquid in contact.

Figure 8 compares the ethanol mole fraction of the permeate as a function of downstream pressure obtained from experiments with the prediction from the modified pore-flow model using all transport parameters listed in Table 4. From the result, there is a fair agreement between the modified pore-flow model and the experimental data. In any case, the model is able to predict the increment of ethanol permeate mole fraction (ethanol selectivity). However, one may see that the influence of downstream pressure on membrane separation can be more complicated, in particular for membranes possessing a high ethanol–water separation factor (e.g., DL_{AG-20-ODR-0.1}), where the modified pore flow shows somewhat of a deviation for predicting the mole fraction of the ethanol permeate at downstream pressures of >1 kPa. This indicates that there may be other separation mechanisms or altered permeate/membrane interactions that facilitate the ethanol transport and meanwhile hinder the water transport. Even though the explicit separation mechanism has yet to be well-understood, this existing phenomenon has been demonstrated in several studies.^{71–73} Ghofar and Kokugan⁷³ reported the same phenomenon that the ethanol can be enriched exceed its vapor–liquid equilibrium composition through hydrophobic porous membranes. They suggested that an increase in downstream pressure toward to the saturation pressure of the dilute ethanol solution could aid the enhancement of the strong interaction between ethanol permeate and hydrophobic membranes.

Another important finding concerns the downstream pressure position that the membranes display the maximal ethanol mole fraction (ethanol selectivity). As shown in Figure 8, there is a close correlation between the total saturation vapor pressure predicted from the modified pore-flow model and the optimal pressure point for each membrane. Previous studies reported that the enriched ethanol on permeate side can be achieved when the downstream pressure is increased and approaches the saturated vapor pressure of the feed mixture. Similarly, this study suggests that the modified pore-flow model is adequate to predict the actual total saturation vapor pressure of the system, which typically corresponds to the chance in achieving the optimal separation selectivity. In other words, this finding suggests operating at the downstream pressure close to the saturated vapor pressure of the system, whereby the location can adequately predicted via the modified pore-flow model.

3.4. Comparison of Pervaporation Performance with the Literature. Figure 9 illustrates the ethanol–water separation performance in terms of separation factor and flux of various membrane materials reported in the literature, including PVDF/nanosilica dual-layer hollow-fiber membranes developed in this study. In the Supporting Information, Table S1 tabulates the status of ethanol–water separation performance for polymeric membranes,^{26,27,29,38,40,74–84} Table S2 shows data for inorganic membranes^{85–91} and Table S3 shows data for mixed-matrix or organic–inorganic membranes.^{29,34–36,38} The detailed information provided in Tables S1–S3 not only supports our claim that this is a pioneer work on developing dual-layer hollow fibers for ethanol recovery while most studies are based on flat-sheet membranes, but also presents a comprehensive survey of various membrane materials ranging from polymers, inorganic membranes, and mixed-matrix or hybrid membranes available in the literature for ethanol recovery. Most polymeric membranes reported in previous studies have a relatively low selectivity with a wide range of permeation flux. Silicalite-1 or hydrophobic zeolite membranes exhibit both high selectivity and flux while the pervaporation performance of mixed-matrix or hybrid membranes, which are mostly silicalite-1/PDMS membranes, is

spatially scattered in the transition gap between both respective materials.

It can be seen that the developed PVDF/nanosilica dual-layer hollow fibers displayed an outstanding ethanol–water separation factor and a sustainable flux, compared to most prior state of the art of polymeric and hybrid membranes. The magnitude of fluxes and separation factors observed with resultant PVDF/nanosilica dual-layer hollow fiber membranes has not been reported in the open literature, especially for polymeric membranes. The best performance observed with a separation factor of 29 and a total flux of $1.1 \text{ kg m}^{-2} \text{ h}^{-1}$ is found in the same region with the separation characteristic of inorganic membranes. With such encouraging separation performance, and together with the benefits of membrane fabrication and process operation at a practical industrial-scale vacuum system, the newly developed PVDF/nanosilica dual-layer hollow fiber can be a promising candidate for ethanol recovery.

4. CONCLUSIONS

Novel PVDF/nanosilica dual-layer hollow fiber membranes with desirable membrane morphology and separation performance for ethanol recovery using the concept of the modified pore-flow model have been developed. The following conclusions can be drawn from the result of the current work:

- (1) By introducing hydrophobic nanosilica with optimizing air-gap distance, take-up speed, and outer-dope flow rate, the desirable membrane morphology, which consists of a thin skin layer of PVDF/silica composite, a highly porous spongelike support structure is successfully fabricated. The resultant membranes possess the mean pore size in nanorange with a relative high surface porosity in the magnitude of 10^2 m^{-1} , and the water contact angle can be as high as 99° . The membranes with a smaller pore size and greater hydrophobicity acquire a better membrane selectivity while the total flux is crucially contributed by the effective surface porosity of the membranes.
- (2) The downstream pressure plays a critical role in controlling penetrant transports and membrane separation performance, in addition to the related morphological and physical properties of membranes, i.e., pore size, surface porosity, and hydrophobicity. By applying downstream pressure close to the optimum total saturation vapor pressure, which can be adequately predicted by the modified pore-flow model, the ethanol enrichment can be accomplished.
- (3) The developed PVDF/nanosilica dual-layer hollow-fiber membranes have ethanol–water separation factors of 8–29 and total fluxes of $1.1\text{--}4.3 \text{ kg m}^{-2} \text{ h}^{-1}$, depending upon tailored membrane morphologies and controlled downstream pressures. In comparison with various types of membranes available in the literature, the accomplished high separation factor of up to 29 and a total flux of $1.1 \text{ kg m}^{-2} \text{ h}^{-1}$ is approachable the separation characteristic of inorganic membranes.

■ APPENDIX A

A.1. Sample Estimation of Pore Size Using Liquid Transport Parameters for Pure Water (A_w/δ) and Pure Ethanol (A_e/δ) Systems. According to the modified pore-flow model,⁴¹ the pore size can be determined using the following equation:

$$r = \left[\left(\frac{A}{\delta} \right) \frac{8\eta_L M}{\rho} \left(\frac{1}{\varepsilon_s/\delta} \right) \right]^{1/2} \quad (\text{A1})$$

For pure water at 50°C : $\rho = 988 \text{ kg m}^{-3}$, $\eta_L = 5.47 \times 10^{-4} \text{ Pa s}$, $M_w = 0.018 \text{ kg mol}^{-1}$. Moreover, the membrane (DL_{AG-20}) has the following properties: $\varepsilon_s/\delta = 6.41 \times 10^2 \text{ m}^{-1}$ (from Table 2) and $A_w/\delta = 5.05 \times 10^{-8} \text{ mol m}^{-2} \text{ s}^{-1} \text{ Pa}^{-1}$ (from Table 4).

Therefore, the pore size obtained for the pure water system is

$$r = \left[(5.05 \times 10^{-8}) \times \frac{8 \times 5.47 \times 10^{-4} \times 0.018}{988} \times \left(\frac{1}{6.41 \times 10^2} \right) \right]^{1/2} = 2.51 \times 10^{-9} \text{ m} = 2.51 \text{ nm} \quad (\text{A2})$$

Similarly, for pure ethanol at 50°C : $\rho = 763 \text{ kg m}^{-3}$, $\eta_L = 6.70 \times 10^{-4} \text{ Pa s}$, $M_e = 0.046 \text{ kg mol}^{-1}$, $\varepsilon_s/\delta = 6.41 \times 10^2 \text{ m}^{-1}$ (from Table 2) and $A_e/\delta = 1.65 \times 10^{-5} \text{ mol m}^{-2} \text{ s}^{-1} \text{ Pa}^{-1}$ (from Table 4).

Thus, the pore size obtained for the pure ethanol system is

$$r = \left[(1.65 \times 10^{-5}) \times \frac{8 \times 6.70 \times 10^{-4} \times 0.046}{763} \times \left(\frac{1}{6.41 \times 10^2} \right) \right]^{1/2} = 9.12 \times 10^{-8} \text{ m} = 91.2 \text{ nm} \quad (\text{A3})$$

A.2. Sample Estimation of Pore Size Using Vapor Transport Parameters for Pure Water (C_w/δ) and Pure Ethanol (C_e/δ) Systems. According to the modified pore-flow model,⁴¹ the pore size can be expressed as

$$r = \frac{3}{2} \left(\frac{C}{\delta} \right) \left(\frac{\pi M}{8RT} \right)^{1/2} \frac{RT}{(\varepsilon_s/\delta)} \quad (\text{A4})$$

For pure water at 50°C : $M_w = 0.018 \text{ kg mol}^{-1}$, $T = 323 \text{ K}$, $R = 8.314 \text{ m}^3 \text{ Pa mol}^{-1} \text{ K}^{-1}$. The membrane (DL_{AG-20}) has the following properties: $\varepsilon_s/\delta = 6.41 \times 10^4 \text{ m}^{-1}$ (from Table 2) and $C_w/\delta = 5.15 \times 10^{-6} \text{ mol m}^{-2} \text{ s}^{-1} \text{ Pa}^{-1}$ (from Table 4).

Hence, the calculated pore size for the pure water system is

$$r = (5.15 \times 10^{-6}) \times \frac{3}{2} \left(\frac{3.14 \times 0.018}{8 \times 8.314 \times 323} \right)^{1/2} \times \frac{(8.314 \times 323)}{(6.41 \times 10^4)} = 5.25 \times 10^{-8} \text{ m} = 52.5 \text{ nm} \quad (\text{A5})$$

For pure ethanol at 50°C : $M_e = 0.046 \text{ kg mol}^{-1}$, $T = 323 \text{ K}$, $R = 8.314 \text{ m}^3 \text{ Pa mol}^{-1} \text{ K}^{-1}$, $\varepsilon_s/\delta = 6.41 \times 10^2 \text{ m}^{-1}$ (from Table 2) and $C_e/\delta = 3.10 \times 10^{-6} \text{ mol m}^{-2} \text{ s}^{-1} \text{ Pa}^{-1}$ (from Table 4).

As a result, the pore size for pure ethanol system is

$$r = (3.10 \times 10^{-6}) \times \frac{3}{2} \left(\frac{3.14 \times 0.046}{8 \times 8.314 \times 323} \right)^{1/2} \times \frac{(8.314 \times 323)}{(6.41 \times 10^2)} = 5.05 \times 10^{-8} \text{ m} = 50.5 \text{ nm} \quad (\text{A6})$$

■ ASSOCIATED CONTENT

S Supporting Information. A literature survey of membrane materials and their pervaporation performance for ethanol recovery includes data for polymeric membranes (Table S1), inorganic membranes (Table S2), and mixed-matrix or organic–inorganic membranes (Table S3). Figure S1 illustrates experimental setup and design for the pervaporation test with a heated permeate line. This information is available free of charge via the Internet at <http://pubs.acs.org/>.

■ AUTHOR INFORMATION

Corresponding Author

*Tel.: 65 6516 6645. Fax: 65 6779 1936. E-mail: chencts@nus.edu.sg.

■ ACKNOWLEDGMENT

The authors would like to thank the Singapore National Research Foundation (NRF) for support through the Competitive Research Program for the project entitled, “New Biotechnology for Processing Metropolitan Organic Wastes into Value-Added Products” (Grant No. R-279-000-311-281). Special thanks are also given to Dr. Natalia Widjojo, Dr. Yan Wang, and Ms. Mei Ling Chua for their valuable comments to this study.

■ NOMENCLATURE

A = liquid transport parameter for a pure component system ($\text{mol m}^{-1} \text{s}^{-1} \text{Pa}^{-1}$)
 A_a = effective membrane area (m^2)
 A_e = liquid transport parameter A of the ethanol component
 A_w = liquid transport parameter A of water components
 B = vapor transport parameter represented the surface flow contribution for a pure component system ($\text{mol m}^{-1} \text{s}^{-1} \text{Pa}^{-2}$)
 B_e = vapor transport parameter B of the ethanol component
 B_w = vapor transport parameter B of water components, respectively
 C = vapor transport parameter represented the Knudsen flow contribution for a pure component system ($\text{mol m}^{-1} \text{s}^{-1} \text{Pa}^{-1}$)
 C_e = vapor transport parameter C of the ethanol component
 C_w = vapor transport parameter C of the water component
 D = outer diameter of the hollow fiber (cm)
 F = total gas permeation rate (mol s^{-1})
 G = gas permeance or gas permeation flux ($\text{mol m}^{-2} \text{Pa}^{-1} \text{s}^{-1}$)
 I_0 = intercept of the plot of G against mean pressures
 J = total mass transferred over collecting time (g)
 l = effective length of the module (cm)
 M = molecular weight (kg mol^{-1})
 M_e = molecular weight of ethanol component (kg mol^{-1})
 M_w = molecular weight of the water component (kg mol^{-1})
 n = number of fibers in one testing module
 P_2 = upstream pressure, pressure at the feed side (or the pore inlet) (Pa)
 P_3 = downstream pressure, pressure at the permeate side (or the pore outlet) (Pa)
 P_* = saturation vapor pressure at the liquid–vapor phase boundary for a pure system (Pa)
 $P_{*,\text{ethanol-water}}$ = total saturation vapor pressure at the liquid–vapor phase boundary for ethanol–water mixture system (Pa)
 P_m = mean pressure (Pa)
 $P_{e,3}$ = partial vapor pressure of the ethanol component at the

permeate side (or the pore outlet) (Pa)
 $P_{w,3}$ = partial vapor pressure of water component at the permeate side (or the pore outlet) (Pa)
 $P_{e,*}$ = partial vapor pressure of the ethanol components in the saturated vapor (Pa)
 $P_{w,*}$ = partial vapor pressure of the water components in the saturated vapor (Pa)
 ΔP = gas pressure difference across the membrane (Pa)
 Q_{Knudsen} = molar flux in the vapor-phase transport govern by Knudsen flow ($\text{mol m}^{-2} \text{s}^{-1}$)
 Q_{liquid} = molar flux in the liquid-phase transport ($\text{mol m}^{-2} \text{s}^{-1}$)
 Q_{surface} = molar flux in the vapor-phase transport govern by surface flow ($\text{mol m}^{-2} \text{s}^{-1}$)
 Q_{total} = total molar flux ($\text{mol m}^{-2} \text{s}^{-1}$)
 r = mean pore size at the selective layer surface (m)
 R = gas constant; $R = 8.314 \text{ m}^3 \text{ Pa mol}^{-1} \text{ K}^{-1}$
 S_0 = slope of the plot of G against mean pressures
 t = collecting time (s or h)
 T = absolute temperature (K)
 W_{total} = total mass flux ($\text{g m}^{-2} \text{s}^{-1}$ or $\text{g m}^{-2} \text{h}^{-1}$)
 X_e = mole fraction of ethanol in the feed
 X_w = mole fraction of water in the feed
 $Y_e, Y_{e,3}$ = mole fraction of ethanol in the permeate side
 $Y_w, Y_{w,3}$ = mole fraction of water in the permeate side

■ GREEK SYMBOLS

$\alpha_{\text{ethanol/water}}$ = ethanol–water separation factor
 δ = entire length of the pore or effective pore length (m)
 ε_s = surface porosity
 η_L = viscosity of liquid (Pa s)
 η_g = viscosity of gas (Pa s)
 ρ = density of liquid (kg m^{-3})
 θ = water contact angle

■ REFERENCES

- (1) Balat, M.; Balat, H.; Oz, C. Progress in bioethanol processing. *Prog. Energy Combust. Sci.* **2008**, *34*, 551.
- (2) Hoekman, S. K. Biofuels in the U.S.-challenges and opportunities. *Renewable Energy* **2009**, *34*, 14.
- (3) Wiesenthal, T.; Leduc, G.; Christidis, P.; Schade, B.; Pelkmans, L.; Govaerts, L.; Georgopoulos, P. Biofuel support policies in Europe: Lessons learnt for the long way ahead. *Renewable Sustainable Energy Rev.* **2009**, *13*, 789.
- (4) Szulczyk, K. R.; McCarl, B. A.; Cornforth, G. Market penetration of ethanol. *Renewable Sustainable Energy Rev.* **2010**, *14*, 394.
- (5) Lynd, L. R.; Cruz, C. H. B. Make way for ethanol. *Science* **2010**, *330*, 1176.
- (6) Somervill, C.; Youngs, H.; Taykor, C.; Davis, S. C.; Long, S. P. Feedstocks for lignocellulosic biofuels. *Science* **2010**, *329*, 790.
- (7) Eggeman, T.; Elander, R. T. Process, economic analysis of pretreatment technologies. *Bioresour. Technol.* **2005**, *96*, 2019.
- (8) Larsson, M.; Zacchi, G. Production of ethanol from dilute glucose solution. A technical-economic evaluation of various refining alternatives. *Bioprocess Eng.* **1996**, *15*, 125.
- (9) Maiorella, B. L. Ethanol. In *Comprehensive Biotechnology*, Vol. 3; Moo-Young, M., Ed.; Pergamon Press: New York, 1985; p 861.
- (10) Vane, L. M. Review: Separation technologies for the recovery and dehydration of alcohols from fermentation broths. *Biofuels, Bioprod. Bioref.* **2008**, *2*, 553.
- (11) Cardona, C. A.; Sánchez, O. J. Fuel ethanol production: process design trends and integration opportunities. *Bioresour. Technol.* **2007**, *98*, 2415.
- (12) Stephanopoulos, G. Challenges in engineering microbes for biofuels production. *Science* **2007**, *315*, 801.

- (13) Huang, Y.; Baker, R. W. *Bioethanol Production Using Pervaporation and Vapour Permeation Membranes*; Presented at the International Congress on Membrane and Membrane Process, Honolulu, HI, 2008.
- (14) Jiang, L. Y.; Wang, Y.; Chung, T. S.; Qiao, X. Y.; Lai, J. Y. Polyimides membranes for pervaporation and biofuels separation. *Prog. Polym. Sci.* **2009**, *34*, 1135.
- (15) Thongsukmak, A.; Sirkar, K. K. Extractive pervaporation to separate ethanol from its dilute aqueous solutions characteristic of ethanol-producing fermentation processes. *J. Membr. Sci.* **2009**, *329*, 119.
- (16) Fleming, H. L.; Slater, C. S. Pervaporation. In *Membrane Handbook*; Ho, W. S., Sirkar, K. K., Eds.; Kluwer Academic Publishers: New York, 1992; p 103.
- (17) Huang, H. J.; Ramaswamy, S.; Tschirner, U. W.; Ramarao, B. V. A review of separation technologies in current and future biorefineries. *Sep. Purif. Technol.* **2008**, *62*, 1.
- (18) Tu, C. Y.; Liu, Y. L.; Lee, K. R.; Lai, J. Y. Hydrophilic surface-grafted poly(tetrafluoroethylene) membranes using in pervaporation dehydration processes. *J. Membr. Sci.* **2006**, *274*, 47.
- (19) O'Brien, D. J.; Roth, L. H.; McAlloon, A. J. Ethanol production by continuous fermentation—pervaporation: A preliminary economic analysis. *J. Membr. Sci.* **2000**, *166*, 105.
- (20) Ding, W. W.; Wu, Y. T.; Tang, X. Y.; Yuan, L.; Xiao, Z. Y. Continuous ethanol fermentation in a closed-circulating system using an immobilized cell coupled with PDMS membrane pervaporation. *J. Chem. Technol. Biotechnol.* **2011**, *86*, 82.
- (21) Vane, L. M. A review of pervaporation for product recovery from biomass fermentation processes. *J. Chem. Technol. Biotechnol.* **2005**, *80*, 603.
- (22) Gonzalez-Velasco, J. R.; Gonzalez-Marcos, J. A.; Lopez-Dehesa, C. Pervaporation of ethanol–water mixtures through poly(1-trimethylsilyl-1-propyne) (PTMSP) membranes. *Desalination* **2002**, *149*, 61.
- (23) Nagase, Y.; Ishihara, K.; Matsui, K. Chemical modification of poly(substituted-acetylene): II. Pervaporation of ethanol/water mixture through poly(1-trimethylsilyl-1-propyne)/poly(dimethylsiloxane) graft copolymer membrane. *J. Polym. Sci., Part B: Polym. Phys.* **1990**, *28*, 377.
- (24) Volkov, V. V.; Fadeev, A. G.; Khotimsky, V. S.; Litvinova, E. G.; Selinskaya, Y. A.; McMillan, J. D.; Kelly, S. S. Effects of synthesis conditions on the pervaporation properties of poly[1-(trimethylsilyl)-1-propyne] useful for membrane bioreactors. *J. Appl. Polym. Sci.* **2004**, *91*, 2271.
- (25) Kazuhiko, I.; Kiyohide, M. Pervaporation of ethanol-water mixture through composite membranes composed of styrene-fluoroalkyl acrylate graft copolymers and crosslinked polydimethylsiloxane membrane. *J. Appl. Polym. Sci.* **1987**, *34*, 437.
- (26) Huang, Y.; Fu, J.; Pan, Y.; Huang, X.; Tang, X. Pervaporation of ethanol aqueous solution by polyphosphazene membranes: Effect of pendant groups. *Sep. Purif. Technol.* **2009**, *66*, 504.
- (27) Takegemi, S.; Yamada, H.; Tusujii, S. Pervaporation of ethanol/water mixture using novel hydrophobic membrane containing polydimethylsiloxane. *J. Membr. Sci.* **1992**, *75*, 93.
- (28) Liu, F.; Liu, L.; Feng, X. Separation of acetone-butanol-ethanol (ABE) from dilute aqueous solutions by pervaporation. *Sep. Purif. Technol.* **2005**, *42*, 273.
- (29) Dobrak, A.; Figoli, A.; Chovau, S.; Galiano, F.; Simone, S.; Vankelecom, I. F. J.; Drioli, E.; Van der Bruggen, B. Performance of PDMS membranes in pervaporation: Effect of silicalite fillers and comparison with SBS membranes. *J. Colloid Interface Sci.* **2010**, *346*, 254.
- (30) Chung, T. S.; Jiang, L. Y.; Kulprathipanja, S. Mixed matrix membranes (MMMs) comprising organic polymers with dispersed inorganic fillers for gas separation. *Prog. Polym. Sci.* **2007**, *32*, 483.
- (31) Kulprathipanja, S.; Nousil, R. W.; Li, N. N. *Separation of fluids by means of mixed matrix membranes in gas permeation*. U.S. Patent 4,740,219, 1998.
- (32) Hennepe, H. J. C. te.; Bargeman, D.; Mulder, M. H. V.; Smolders, C. A. Zeolite-filled silicone rubber membranes Part 1. Membrane preparation and pervaporation results. *J. Membr. Sci.* **1987**, *35*, 39.
- (33) Jia, M. D.; Peinemann, K. V.; Behling, R. D. Preparation and characterization of thin-film zeolite-PDMS composite membranes. *J. Membr. Sci.* **1992**, *73*, 119.
- (34) Vane, L. M.; Namboodiri, V. V.; Bowen, T. C. Hydrophobic zeolite-silicone rubber mixed matrix membranes for ethanol-water separation: Effect of zeolite and silicone component selection on pervaporation performance. *J. Membr. Sci.* **2008**, *308*, 230.
- (35) Yi, S.; Su, Y.; Wan, Y. Preparation and characterization of vinyltriethoxysilane (VTES) modified silicalite-1/PDMS hybrid pervaporation performance and its application in ethanol separation from dilute aqueous solution. *J. Membr. Sci.* **2010**, *360*, 341.
- (36) Huang, Y.; Zhang, P.; Fu, J.; Zhou, Y.; Huang, X.; Tang, X. Pervaporation of ethanol aqueous solution by polydimethylsiloxane/polyphosphazene nanotube nanocomposite membranes. *J. Membr. Sci.* **2009**, *339*, 85.
- (37) Vankelecom, I. F. J.; Kinderen, J. D.; Dewitte, B. M.; Uytterhoeven, J. B. Incorporation of hydrophobic porous fillers in PDMS membranes for use in pervaporation. *J. Phys. Chem. B* **1997**, *101*, 5182.
- (38) Claes, S.; Vandecasteele, P.; Mullens, S.; Leysen, R.; Sitter, K. D.; Andersson, A.; Maurer, F. H. J.; Van den Rul, H.; Peeters, R.; Van Bael, M. K. High flux composite PTMSP-silica nanohybrid membranes for the pervaporation of ethanol/water mixtures. *J. Membr. Sci.* **2010**, *351*, 160.
- (39) Peng, P.; Shi, B.; Lan, Y. A review of membrane materials for ethanol recovery by pervaporation. *Sep. Sci. Technol.* **2011**, *46*, 234.
- (40) Sukitpaneenit, P.; Chung, T. S. Molecular design of the morphology and pore size of PVDF hollow fiber membranes for ethanol-water separation employing the modified pore-flow concept. *J. Membr. Sci.* **2011**, *374*, 67.
- (41) Sukitpaneenit, P.; Chung, T. S.; Jiang, L. Y. Modified pore-flow model for pervaporation mass transport in PVDF hollow fiber membranes for ethanol-water separation. *J. Membr. Sci.* **2010**, *362*, 393.
- (42) Feng, X.; Huang, R. Y. M. Liquid separation by membrane pervaporation: A review. *Ind. Eng. Chem. Res.* **1997**, *36*, 1048.
- (43) Wijmans, J. G.; Baker, R. W. The solution-diffusion model: A review. *J. Membr. Sci.* **1995**, *107*, 1.
- (44) Bonyadi, S.; Chung, T. S. Flux enhancement in membrane distillation by fabrication of dual layer hydrophilic-hydrophobic hollow fiber membranes. *J. Membr. Sci.* **2007**, *306*, 134.
- (45) Wang, K. Y.; Foo, S. W.; Chung, T. S. Mixed matrix PVDF hollow fiber membranes with nanoscale pores for desalination through direct contact membrane distillation. *Ind. Eng. Chem. Res.* **2009**, *48*, 4474.
- (46) Teoh, M. M.; Chung, T. S. Membrane distillation with hydrophobic macrovoid-free PVDF-PTFE hollow fiber membranes. *Sep. Purif. Technol.* **2009**, *66*, 229.
- (47) Hashim, N. A.; Liu, Y.; Li, K. Preparation of PVDF hollow fiber membranes using SiO₂ particles: The effect of acid and alkali treatment on the membrane performances. *Ind. Eng. Chem. Res.* **2011**, *50*, 3035.
- (48) Shen, H. L.; Liao, H.; Xiao, C. F. Formation mechanism and properties of polyvinylidene fluoride (PVDF)/nano-silica hybrid membranes. *Adv. Mater. Res.* **2010**, *123–125*, 93.
- (49) Yu, L. Y.; Xu, Z. L.; Shen, H. M.; Yang, H. Preparation and characterization of PVDF–SiO₂ composite hollow fiber UF membrane by sol–gel method. *J. Membr. Sci.* **2009**, *337*, 257.
- (50) Cao, X.; Ma, J.; Shi, X.; Ren, Z. Effect of TiO₂ nanoparticle size on the performance of PVDF membrane. *Appl. Surf. Sci.* **2006**, *253*, 2003.
- (51) Oh, S. J.; Kim, N.; Lee, Y. T. Preparation and characterization of PVDF/TiO₂ organic-inorganic composite membranes for fouling resistance improvement. *J. Membr. Sci.* **2009**, *345*, 13.
- (52) Yan, L.; Li, Y. S.; Xiang, C. B. Preparation of poly(vinylidene fluoride) (PVDF) ultrafiltration membrane modified by nano-sized alumina (Al₂O₃) and its antifouling research. *Polymer* **2005**, *46*, 7701.
- (53) Bottino, A.; Capannelli, G.; Comite, A. Preparation and characterization of novel porous PVDF–ZrO₂ composite membrane. *Desalination* **2002**, *146*, 35.
- (54) Jiang, L. Y.; Chung, T. S.; Kulprathipanja, S. Fabrication of mixed matrix hollow fibers with intimate polymer–zeolite interface for gas separation. *AIChE J.* **2006**, *52*, 2898.
- (55) Li, Y.; Chung, T. S.; Huang, Z.; Kulprathipanja, S. Dual-layer polyethersulfone (PES)/BTDA-TDI/MDI co-polyimide (P84) hollow

- fiber membranes with a submicron PES-zeolite beta mixed matrix dense-selective layer for gas separation. *J. Membr. Sci.* **2006**, *277*, 28.
- (56) Greenlaw, F. W.; Prince, W. D.; Shelden, R. A.; Thompson, E. V. Dependence of diffusive permeation rates on upstream and downstream pressures. II. Two component permeate. *J. Membr. Sci.* **1977**, *2*, 333.
- (57) Huang, R. Y. M.; Rhim, J. W. Separation characteristics of pervaporation membrane separation processes. In *Pervaporation Membrane Separation Processes*; Huang, R. Y. M., Ed.; Elsevier Science Publishers B.V.: Amsterdam, The Netherlands, 1991.
- (58) Ten, P. K.; Field, R. W. Organophilic pervaporation: an engineering science analysis of component transport and the classification of behavior with reference to the effect of permeate pressure. *Chem. Eng. Sci.* **2000**, *55*, 1425.
- (59) Vallieres, C.; Favre, E.; Roizard, D.; Bindelle, J.; Sacco, D. New insights into pervaporation mass transport under increasing downstream pressure conditions: critical role of inert gas entrance. *Ind. Eng. Chem. Res.* **2001**, *40*, 1559.
- (60) Wang, Y.; Chung, T. S.; Neo, B. W.; Gruender, M. Processing and engineering of pervaporation dehydration of ethylene glycol via dual-layer polybenzimidazole (PBI) /polyetherimide (PEI) Membranes. *J. Membr. Sci.* **2011**, *378*, 339.
- (61) Forny, L.; Saleh, K.; Denoyel, R.; Pezron, I. Contact angle assessment of hydrophobic silica nanoparticles related to the mechanisms of dry water formation. *Langmuir* **2010**, *26*, 2333.
- (62) Sukitpaneenit, P.; Chung, T. S. Molecular elucidation of morphology and mechanical properties of PVDF hollow fiber membranes from aspects of phase inversion, crystallization and rheology. *J. Membr. Sci.* **2009**, *340*, 192.
- (63) Li, D.; Chung, T. S.; Wang, R. Morphological aspects and structure control of dual-layer asymmetric hollow fiber membranes formed by a simultaneous co-extrusion approach. *J. Membr. Sci.* **2004**, *243*, 155.
- (64) Henis, J. M. S.; Tripodi, M. K. Composite hollow fiber membranes for gas separation: The resistance model approach. *J. Membr. Sci.* **1981**, *8*, 233.
- (65) Li, K.; Kong, J. F.; Wang, D.; Teo, W. K. Tailor-made asymmetric PVDF hollow fiber for soluble gas removal. *AIChE J.* **1999**, *45*, 1211.
- (66) Jiang, L. Y.; Chung, T. S.; Rajagopalan, R. Dehydration of alcohols by pervaporation through polyimide Matrimid asymmetric hollow fibers with various modifications. *Chem. Eng. Sci.* **2008**, *63*, 204.
- (67) Smith, J. M.; Van Ness, H. C.; Abbott, M. M. *Introduction to Chemical Engineering Thermodynamics*; McGraw-Hill: Singapore, 2005.
- (68) Matsuura, T. *Synthetic Membranes and Membrane Separation Processes*; CRC Press: Boca Raton, FL, 1993.
- (69) Okada, T.; Matsuura, T. A new transport model for pervaporation. *J. Membr. Sci.* **1991**, *59*, 133.
- (70) Sharma, A.; Thampi, S. P.; Suggala, S. V.; Bhattacharya, P. K. Pervaporation from a dense membrane: Roles of permeant-membrane interactions, Kelvin effect, and membrane swelling. *Langmuir* **2004**, *20*, 4708.
- (71) Hoffmann, E.; Pfenning, D. M.; Philippsen, E.; Schwahn, P.; Sieber, M.; When, R.; Woermann, D.; Wiedner, G. Evaporation of alcohol/water mixtures through hydrophobic porous membranes. *J. Membr. Sci.* **1987**, *34*, 199.
- (72) Kokugan, T.; Kaseno; Yoshimoto, E.; Kikukawa, H. A consideration of pervaporation by porous hydrophobic membranes for dilute ethanol solution. *J. Chem. Eng. Jpn.* **1998**, *31*, 153.
- (73) Ghofar, A.; Kokugan, T. The pervaporation mechanism of dilute ethanol solution by hydrophobic porous membranes. *Biochem. Eng. J.* **2004**, *18*, 235.
- (74) Moermans, B.; Beuckelaer, W. D.; Vankelecom, I. F. J.; Ravishankar, R.; Martens, J. A.; Jacobs, P. A. Incorporation of nano-sized zeolites in membranes. *Chem. Commun.* **2000**, *24*, 2467.
- (75) Luo, Y.; Tan, S.; Wang, H.; Wu, F.; Liu, X.; Li, L.; Zhang, Z. PPMS composite membranes for the concentration of organics from aqueous solutions by pervaporation. *Chem. Eng. J.* **2008**, *137*, 496.
- (76) Li, L.; Xiao, Z.; Tan, S.; Pu, L.; Zhang, Z. Composite PDMS membrane with high flux for the separation of organics from water by pervaporation. *J. Membr. Sci.* **2004**, *243*, 177.
- (77) Shi, E.; Huang, W.; Xiao, Z.; Li, D.; Tang, M. Influence of binding interface between active and support layers in composite PDMS membranes on permeation performance. *J. Appl. Polym. Sci.* **2007**, *104*, 2468.
- (78) Guo, J.; Zhang, G.; Wu, W.; Ji, S.; Qin, Z.; Liu, Z. Dynamically formed inner skin hollow fiber polydimethylsiloxane/polysulfone composite membrane for alcohol permselective pervaporation. *Chem. Eng. J.* **2010**, *158*, 558.
- (79) Zhan, X.; Li, J.; Huang, J.; Chen, C. Enhanced pervaporation performance of multi-layer PDMS/PVDF composite membrane for ethanol recovery from aqueous solution. *Appl. Biochem. Biotechnol.* **2010**, *160*, 632.
- (80) Xiangli, F.; Wei, W.; Chen, Y.; Jin, W.; Xu, N. Optimization of preparation conditions for polydimethylsiloxane (PDMS)/ceramic composite pervaporation membranes using response surface methodology. *J. Membr. Sci.* **2008**, *311*, 23.
- (81) Krea, M.; Roizard, D.; Moulaï-Mostefa, N.; Sacco, D. New copolyimide membranes with high siloxane content designed to remove polar organics from water by pervaporation. *J. Membr. Sci.* **2004**, *241*, 55.
- (82) Liang, L.; Ruckenstein, E. Pervaporation of ethanol-water mixtures through polydimethylsiloxane-polystyrene interpenetrating polymer network supported membranes. *J. Membr. Sci.* **1996**, *114*, 227.
- (83) Nagase, Y.; Takamura, Y.; Matsui, K. Chemical modification of poly(substituted-acetylene). V. Alkylsilylation of poly(1-trimethylsilyl-1-propyne) and improved liquid separating property at pervaporation. *J. Appl. Polym. Sci.* **1991**, *42*, 185.
- (84) Gonzalez-Marcos, J. A.; Lopez-Dehesa, C.; Gonzales-Velasco, J. R. Effect of operation conditions in the pervaporation of ethanol-water mixtures with poly(1-trimethylsilyl-1-propyne) membranes. *J. Appl. Polym. Sci.* **2004**, *94*, 1395.
- (85) Sano, T.; Yanagishita, H.; Kiyozumi, Y.; Mizukami, F.; Haraya, K. Separation of ethanol/water mixture by silicalite membrane on pervaporation. *J. Membr. Sci.* **1994**, *95*, 221.
- (86) Shen, D.; Xiao, W.; Yang, J.; Chu, N.; Lu, J.; Yin, D.; Wang, J. Synthesis of silicalite-1 membrane with two silicon source by secondary growth method and its pervaporation performance. *Sep. Purif. Technol.* **2011**, *76*, 308.
- (87) Lin, X.; Chen, X.; Kita, H.; Okamoto, K. Synthesis of silicalite tubular membranes by in situ crystallization. *AIChE J.* **2003**, *49*, 237.
- (88) Lin, X.; Kita, H.; Okamoto, K. I. Silicalite membrane preparation, characterization and separation performance. *Ind. Eng. Chem. Res.* **2001**, *40*, 4069.
- (89) Sano, T.; Hasegawa, M.; Ejiri, S.; Kawakami, Y.; Yanagishita, H. Improvement of the pervaporation performance of silicalite membranes by modification with a silane coupling reagent. *Microporous Mater.* **1995**, *5*, 179.
- (90) Bowen, T. C.; Kalipci, H.; Falconer, J. L.; Noble, R. D. Pervaporation of organic/water mixtures through B-ZSM-5 zeolite membranes on monolith supports. *J. Membr. Sci.* **2003**, *215*, 235.
- (91) Sebastian, V.; Motuzas, J.; Dirrix, R. W. J.; Terpstra, R. A.; Mallada, R.; Julbe, A. Synthesis of capillary titaniosilicalite TS-1 ceramic membranes by MW-assisted hydrothermal heating for pervaporation application. *Sep. Purif. Technol.* **2010**, *75*, 249.